

Revealing the Substructure of Single-Walled Carbon Nanotube Fibers

Yuhuang Wang,^{†,‡} Lars M. Ericson,^{†,§} Carter Kittrell,^{†,‡} Myung Jong Kim,^{†,§}
 Hongwei Shan,^{†,‡} Hua Fan,^{†,§} Steve Ripley,[†] Sivarajan Ramesh,[†] Robert H. Hauge,^{†,‡}
 W. Wade Adams,[†] Matteo Pasquali,^{*,†,||} and Richard E. Smalley^{*,†,‡,§}

Center for Nanoscale Science and Technology, Carbon Nanotechnology Laboratory, and Departments of Chemistry, Physics, and Chemical & Biomolecular Engineering, Rice University, MS-100, Post Office Box 1892, Houston, Texas 77251-1892

Received August 17, 2005. Revised Manuscript Received October 11, 2005

Single-walled carbon nanotubes (SWNTs) uniquely combine characteristics of polymers (e.g., they are molecules composed of repeat units) as well as nanoscale colloids (e.g., they are extremely stiff); because of these characteristics, they may qualify as the ideal building blocks for the long-sought Staudinger's "continuous crystal." To this end, neat SWNT fibers have been produced by wet-spinning concentrated dispersions of 6–10 wt % SWNTs in 102% H₂SO₄. A unique protocol that combined UV–ozone dry chemical etching and cryoultramicrotoming was developed to directly visualize the internal voids, alignment, and composition of these SWNT neat fibers. A substructure of large aligned SWNT ropes, 200–500 nm in diameter, was revealed throughout the fibers. This substructure may be linked to the SWNT spaghetti, threadlike liquid-crystalline domains observed in dispersions of SWNTs in H₂SO₄.

1. Introduction

Since their discovery,^{1,2} single-walled carbon nanotubes (SWNTs) have continued to surprise researchers with their extraordinary properties. Individual metallic SWNTs conduct electricity better than copper,³ while semiconducting SWNTs possess a carrier mobility higher than that of silicon.⁴ In addition, SWNTs have a thermal conductivity close to that of diamond⁵ and are stronger than high-performance steel^{6,7} at only $\sim 1/6$ the density. However, in comparison, aggregated SWNT buckypaper exhibits marginal properties.^{8–10} These superior "molecular" properties are largely compromised in

the bulk by structural defects (voids, porosity, gaps, disconnects, etc.) arising from the tangled arrangement and loose packing of SWNTs. To maximally retain the extraordinary properties of individual SWNTs in bulk materials, it is essential to develop a continuous, crystalline fiber in which SWNTs are densely packed in an ordered array, similar to the long-sought Staudinger's "continuous crystal" of polymers.^{11,12} Because of their potential for a wide spectrum of applications as high-strength, lightweight, thermally and electrically conducting structural elements, SWNT fibers are currently undergoing intense research and development. To date, many variations on SWNT fibers have been produced,¹³ including composite fibers,^{14,15} fibers comprising surfactants and polymers^{16–19} or DNA,²⁰ neat fibers,^{21–25} and strands²⁶

* Corresponding authors: e-mail mp@rice.edu (M.P.), smalley@rice.edu (R.E.S.).

[†] Center for Nanoscale Science and Technology, Carbon Nanotechnology Laboratory.

[‡] Department of Chemistry.

[§] Department of Physics.

^{||} Department of Chemical & Biomolecular Engineering.

- (1) Iijima, S.; Ichihashi, T. *Nature* **1993**, *363*, 603–15.
- (2) Bethune, D. S.; Kiang, C. H.; deVries, M. S.; Gorman, G.; Savoy, R.; Vazquez, J.; Beyers, R. *Nature* **1993**, *363*, 605–7.
- (3) Tans, S. J.; Devoret, M. H.; Dai, H. J.; Thess, A.; Smalley, R. E.; Geerligs, L. J.; Dekker, C. *Nature* **1997**, *386*, 474–477.
- (4) Duerkop, T.; Getty, S. A.; Cobas, E.; Fuhrer, M. S. *Nano Lett.* **2004**, *4*, 35–39.
- (5) Che, J.; Cagin, T.; Goddard, W. A., III. *Nanotechnology* **2000**, *11*, 65–69.
- (6) Krishnan, A.; Dujardin, E.; Ebbesen, T. W.; Yianilos, P. N.; Treacy, M. M. J. *Phys. Rev. B* **1998**, *58*, 14013–14019.
- (7) Yu, M.-F.; Files, B. S.; Arepalli, S.; Ruoff, R. S. *Phys. Rev. Lett.* **2000**, *84*, 5552–5555.
- (8) Rinzler, A. G.; Liu, J.; Dai, H.; Nikolaev, P.; Huffman, C. B.; Rodriguezmacias, F. J.; Boul, P. J.; Lu, A. H.; Heymann, D.; Colbert, D. T.; Lee, R. S.; Fischer, J. E.; Rao, A. M.; Eklund, P. C.; Smalley, R. E. *Appl. Phys. A* **1998**, *67*, 29–37.
- (9) Hone, J.; Whitney, M.; Piskoti, C.; Zettl, A. *Phys. Rev. B* **1999**, *59*, R2514–R2516.
- (10) Baughman, R. H.; Cui, C. X.; Zakhidov, A. A.; Iqbal, Z.; Barisci, J. N.; Spinks, G. M.; Wallace, G. G.; Mazzoldi, A.; De Rossi, D.; Rinzler, A. G.; Jaszchinski, O.; Roth, S.; Kertesz, M. *Science* **1999**, *284*, 1340–1344.

- (11) Staudinger, H. in *Die Hochmolekularen Organischen Verbindungen*. Springer: Berlin, 1932; p 111.
- (12) Jiang, H.; Adams, W. W.; Eby, R. K. In *Materials Science & Technology*; Thomas, E. L., Ed.; VCH Publishers Inc.: New York, 1993; Vol. 12, pp 597–652.
- (13) Davis, V. A.; Pasquali, M. In *Nanoengineering of Structural, Functional and Smart Materials*; Schulz, M. J., Kelkar, A. D., Sundaresan, M. J., Eds.; CRC Press: Boca Raton, FL, 2005.
- (14) Andrews, R.; Jacques, D.; Rao, A. M.; Rantell, T.; Derbyshire, F.; Chen, Y.; Chen, J.; Haddon, R. C. *Appl. Phys. Lett.* **1999**, *75*, 1329–1331.
- (15) Kumar, S.; Dang, T. D.; Arnold, F. E.; Bhattacharyya, A. R.; Min, B. G.; Zhang, X.; Vaia, R. A.; Park, C.; Adams, W. W.; Hauge, R. H.; Smalley, R. E.; Ramesh, S.; Willis, P. A. *Macromolecules* **2002**, *35*, 9039–9043.
- (16) Vigolo, B.; Penicaud, A.; Coulon, C.; Sauder, C.; Pailler, R.; Journet, C.; Bernier, P.; Poulin, P. *Science* **2000**, *290*, 1331–1334.
- (17) Dalton, A. B.; Collins, S.; Munoz, E.; Razal, J. M.; Ebron, V. H.; Ferraris, J. P.; Coleman, J. N.; Kim, B. G.; Baughman, R. H. *Nature* **2003**, *423*, 703.
- (18) Badaire, S.; Pichot, V.; Zakri, C.; Poulin, P.; Launois, P.; Vavro, J.; Guthy, C.; Chen, M.; Fischer, J. E. *J. Appl. Phys.* **2004**, *96*, 7509–7513.
- (19) Poulin, P.; Vigolo, B.; Launois, P. *Carbon* **2002**, *40*, 1741–1749.
- (20) Barisci, J. N.; Tahhan, M.; Wallace, G. G.; Badaire, S.; Vaugien, T.; Maugey, M.; Poulin, P. *Adv. Funct. Mater.* **2004**, *14*, 133–138.

consisting solely of SWNTs. Compared to entangled mats and buckypapers, these fibers have shown more ordered structures, along with notable improvements in mechanical and transport properties. However, they still fall short of the theoretical properties of individual SWNTs. Further improvements will rely on the ability to pack SWNTs in a dense and ordered fashion. To this end, structural characterization of these SWNT fibers is essential.

The structure of SWNT fibers is routinely characterized by scanning electron microscopy (SEM), polarized Raman spectroscopy,^{21–27} and X-ray diffraction (XRD).^{18,19,23,24,27,28} However, Raman and XRD provide information only about the bulk alignment of SWNTs, and SEM is limited to surface characterization. Moreover, light penetrates for less than 1 μm in closely packed arrays of SWNTs, effectively restricting Raman analysis to the fiber skin. These methods do not reveal the internal structural defects (i.e., voids, porosity, composition), which cause mechanical failures and poor conductivities, nor the fiber cross section, whose area is essential for accurately deriving intrinsic dimensionless material properties (e.g., Young's modulus, conductivity). Here, we describe a microtoming technique for cross-sectioning SWNT fibers, and two complementary controlled-etching approaches to directly visualize internal structures and void fractions. The sample neat SWNT fibers were spun from concentrated SWNT/sulfuric acid dispersions via wet spinning.^{22–24,29} Throughout the fibers, we observed prevailing superrope substructures 200–500 nm in diameter. Interestingly, the diameter of the superrope substructures is comparable to that of SWNT “spaghetti” —threadlike liquid crystalline domains found in biphasic (isotropic/liquid crystalline) SWNT/H₂SO₄ dispersions²²—and may be linked to the starting liquid crystalline phase.

2. Experimental Methods

2.1. Fiber Spinning. The continuous, neat SWNT fibers were spun from a concentrated dispersion of SWNTs in H₂SO₄ via an industrially viable wet-jet solution-spinning approach. The details

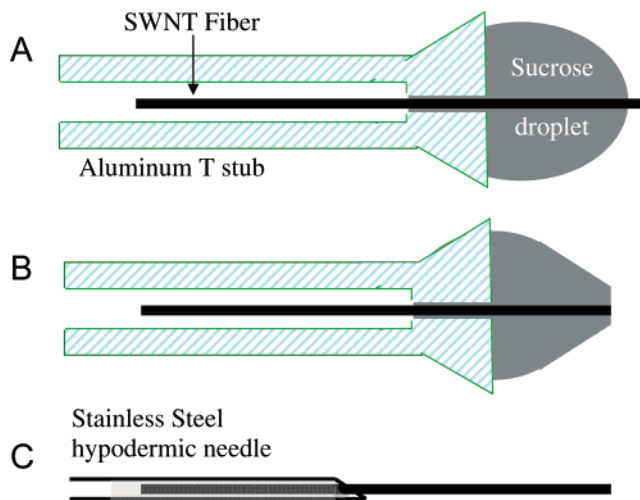


Figure 1. Schematic illustration of the fiber microtoming process: (A) place a drop of 2.3 M sucrose solution on a T-shaped aluminum stub, insert a 6–10 mm fiber through the hole, and freeze to $-100\text{ }^{\circ}\text{C}$; (B) trim the tip of the frozen sucrose droplet into a trapezoid shape that is centered on the fiber, followed by microtoming with a diamond knife; (C) after the desired cross-sections are obtained, recover the microtomed fiber intact and mount the fiber into a stainless steel hypodermic needle, with the microtomed end protruding 2–3 mm.

of this process have been described elsewhere.^{22,24,28–30} Briefly, 4–10 wt % purified high pressure CO (HiPco) materials were mixed with 102% sulfuric acid (2 wt % excess SO₃) to form a liquid crystalline dispersion.²² This ordered SWNT dispersion was then extruded through a small orifice into a coagulant without any extensional drawing.

For this study, fibers were spun from two sample concentrations, 6 and 10 wt % SWNT in 102% sulfuric acid. For 6 wt %, the mixing was carried out at 100 $^{\circ}\text{C}$ for 72 h in a Daga double helix mixer. For 10 wt %, samples were premixed by hand with a mortar and pestle before transfer to the mixer. Both resulted in a well-mixed, viscous, homogeneous, black paste with polydomain birefringent morphology²² and minor degrees of extensibility. This paste was loaded into a stainless steel syringe with a 25 mm long, 125 μm inner diameter stainless steel needle. During the entire sample mixing, transfer, and loading process, the sample was kept under dry argon to avoid phase separation caused by moisture.²² The syringe was then secured in a vertically mounted Harvard Apparatus remote 44 syringe pump, and the fiber was extruded directly into a diethyl ether coagulation bath. The fiber samples were collected from the bath by hand and allowed to dry in air.

2.2. Cryomicrotoming for the Fiber Cross Section. To obtain the cross section, a SWNT fiber was microtomed following a process essentially similar to conventional microtoming. However, because of the high aspect ratio and the need to microtome perpendicular to the fiber axis, a special sample preparation was used to ensure recovery of the samples.

By use of tweezers, a piece of the neat SWNT fiber, approximately 10 mm in length, was inserted into a hole through a “T-shaped” aluminum stub, leaving one end protruding. A drop of 2.3 M sucrose solution was placed on the stub (Figure 1), frozen to $-100\text{ }^{\circ}\text{C}$ in a cryoultramicrotoming stage (Leica Ultracut 125), trimmed into a small trapezoid shape with the fiber in the center, and microtomed perpendicular to the fiber axis with a 35 $^{\circ}$ diamond knife (DiATOME). The part of the fiber deformed by the tweezers was trimmed off. The fiber was fed at 100 nm steps and microtomed

- (21) Gommans, H. H.; Alldredge, J. W.; Tashiro, H.; Park, J.; Magnuson, J.; Rinzler, A. G. *J. Appl. Phys.* **2000**, *88*, 2509–2514.
- (22) Davis, V. A.; Ericson, L. M.; Parra-Vasquez, A. N. G.; Fan, H.; Wang, Y.; Prieto, V.; Longoria, J. A.; Ramesh, S.; Saini, R. K.; Kittrell, C.; Billups, W. E.; Adams, W. W.; Hauge, R. H.; Smalley, R. E.; Pasquali, M. *Macromolecules* **2004**, *37*, 154–160.
- (23) Ericson, L. M.; Fan, H.; Peng, H.; A., D. V.; Zhou, W.; Sulpizio, J.; Wang, Y.; Booker, R.; Vavro, J.; Guthy, C.; Parra-Vasquez, A. N. G.; Kim, M. J.; Ramesh, S.; Saini, R. K.; Kittrell, C.; Lavin, G.; Schmidt, H.; Adams, W. W.; Billups, W. E.; Pasquali, M.; Hwang, W. F.; Hauge, R. H.; Fischer, J. E.; Smalley, R. E. *Science* **2004**, *305*, 1447–1450.
- (24) Zhou, W.; Vavro, J.; Guthy, C.; Winey, K. I.; Fischer, J. E.; Ericson, L. M.; Ramesh, S.; Saini, R.; Davis, V. A.; Kittrell, C.; Pasquali, M.; Hauge, R. H.; Smalley, R. E. *J. Appl. Phys.* **2004**, *95*, 649–655.
- (25) Li, Y.-L.; Kinloch, I. A.; Windle, A. H. *Science* **2004**, *304*, 276–278.
- (26) Zhu, H. W.; Xu, C. L.; Wu, D. H.; Wei, B. Q.; Vajtai, R.; Ajayan, P. M. *Science* **2002**, *296*, 884–886.
- (27) Wei, B.; Vajtai, R.; Choi, Y. Y.; Ajayan, P. M.; Zhu, H.; Xu, C.; Wu, D. *Nano Lett.* **2002**, *2*, 1105–1107.
- (28) Zhou, W.; Winey, K. I.; Fischer, J. E.; Ramesh, S.; Saini, R. K.; Ericson, L. M.; Davis, V. A.; Pasquali, M.; Hauge, R. H.; Smalley, R. E. *Mater. Res. Soc. Symp. Proc.* **2002**, *740*, 429–434.
- (29) Ericson, L. M. Macroscopic Neat Single-Wall Carbon Nanotube Fibers. PhD Thesis, Rice University, Houston, TX, 2003.

- (30) Ramesh, S.; Ericson, L. M.; Davis, V. A.; Saini, R. K.; Kittrell, C.; Pasquali, M.; Billups, W. E.; Adams, W. W.; Hauge, R. H.; Smalley, R. E. *J. Phys. Chem. B* **2004**, *108*, 8794–8798.

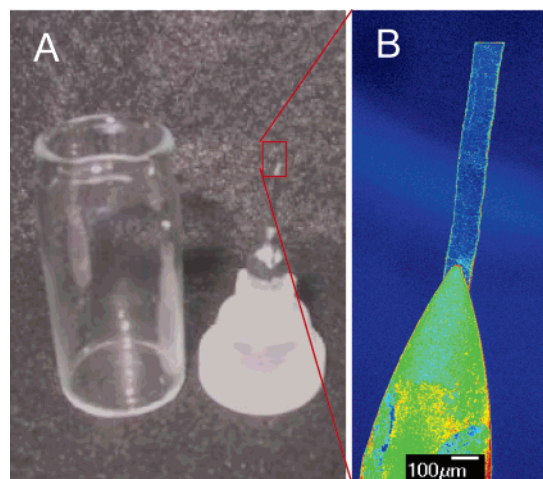


Figure 2. Microtomed SWNT fiber mounted on a stainless steel hypodermic needle. The needle is on a plastic Luer-lock plugged in a forensic sample container.

at a knife speed of 1.0 mm/s until two consecutive slices showed the same complete cross section of the fiber in an optical microscope. After microtoming, the remaining fiber was recovered intact, rinsed with deionized water to remove sucrose, and then mounted into a 26-gauge stainless steel hypodermic needle (Fisher Scientific), with the microtomed end protruding 2–3 mm for subsequent processing. Because the fiber readily adhered to wet surfaces, it could be picked up with a wet rod and inserted into the needle. This procedure avoids damaging the fiber with tweezers. To secure the fiber and avoid charging in the SEM, the needle was filled with a conductive silver paint (Leitsilber 200, Ted Pella) before the fiber was mounted. The capillary action ensured a long path of intimate contact between the fiber and the needle and minimum exposure of silver paint, thereby avoiding potential silver contamination.

Figure 2 shows a microtomed fiber mounted in a hypodermic needle. The fiber could be mounted repeatedly in the same position and orientation by using the angled tip of the hypodermic needle as a convenient reference.

2.3. Etching SWNTs with a Supersonic Jet of Atomic Oxygen.

The microtomed cross section was usually covered with a thin combed layer of SWNTs, as discussed below. This combed layer had to be removed uniformly in order to reveal the internal fiber composition. We found that atomic oxygen, in particular singlet atomic oxygen, O (¹D), was ideally suited for homogeneous etching of SWNTs. O (¹D) is extremely reactive; it relaxes to the triplet state (³P) after about five collisions with O₂ and other molecules.³¹ To create an efficient atomic oxygen source, we designed a supersonic jet of atomic oxygen by combining a conventional supersonic jet with UV–ozone photodissociation. A supersonic jet of O₃ was photodissociated into atomic oxygen within the so-called “zone of silence.”³² Because molecules within the “zone of silence” behave as if they were in a vacuum, the oxygen atoms continue along the beam path without collisions, surviving until they hit the SWNT fiber (Figure 3).

Our custom supersonic jet system consists of a benchtop ozone generator (Yanco Industries), a supersonic cell made of a 2.75-in. Conflat flange cube, a KrF excimer laser (GAM Laser, Inc.) with pulsed output of 248 nm UV light, and a mechanical pump with a throughput of 30 L/s. O₂ (0.25 L/min) was passed through the zone

generator at 1 atm to produce 2.55 mol % O₃. The resulting O₃/O₂ mixture was then expanded into the supersonic cell through a Teflon nozzle (0.50 mm orifice) to form a supersonic jet. Upon exiting the nozzle, the supersonic jet was crossed by the pulsed laser beam with a beam size of 4 mm × 8 mm. The tip of the microtomed fiber was positioned within the zone of silence but above the upper edge of the laser beam. The laser was operated at a frequency of 250 Hz and a light intensity of 8.6×10^{16} photons/cm² per pulse. Typically, $\sim 4 \times 10^6$ pulses were necessary for complete removal of the combed SWNT layer. The low-duty cycle of the laser left most of the ozone undissociated (see Supporting Information).

As a complementary approach, SWNT fibers were oxidized at elevated temperatures (800–950 °C) with an O₂ pressure on the order of 1 mTorr. The SWNT fibers were heated to the desired temperature in an oven or with an Ar⁺ (λ 488 nm) laser beam. Experiments were carried out at different oxygen partial pressures for comparison.

All fiber samples were characterized with a field emission SEM (JEOL 6500F) without applying any metal coating.

3. Results and Discussion

3.1. SWNT Fiber Microtoming.

Crude methods of cross-sectioning a SWNT fiber, such as breaking with a pair of tweezers, liquid N₂ fracturing, or cutting with scissors, severely disturbed the axial alignment of SWNTs, leaving behind a tangled, fibrous, and rough sample. However, microtoming with an atomically sharp diamond knife produced a fairly flat surface with a well-defined fiber cross section.

Figure 4 shows SEM images of a microtomed fiber. Microtoming revealed the overall cross section of the fiber, which offers important engineering and compositional insights. For example, under unoptimized process conditions, fibers with dog-bone cross sections (Figure 4A) were obtained, probably due to rapid formation of a rigid skin during coagulation, as well as excessively rapid evaporation of the coagulant upon removal of the fibers from the bath.²⁹ The cross section is also important for determining accurately intrinsic material properties, such as tensile strength, Young’s modulus, density, and transport conductivity, both thermal and electrical.^{23,26} Microtoming also revealed internal features, such as voids, which are probably the main structural defects that cause the fibers’ mechanical failure. Similar cross sections were obtained consistently by ultramicrotoming at room temperature or by a focused gallium ion beam.³³ The cutting procedure did not affect significantly the cross section of the fibers, indicating that the knife did not induce appreciable macroscopic deformation. Higher magnification SEM images (Figure 4B–D) show that the diamond knife did not cut the tubes. Instead, the knife combed the fibrils along the cutting direction, producing a 20–50 nm thick layer of SWNT ropes with a high degree of alignment. Figure 5 shows clearly that, at the cut edge of the microtomed fiber, the fibrils were bent along the cutting direction. On rare occasions, SWNTs were found broken or pulled out, resulting in a rougher surface. Microtoming with a glass knife or larger final feeding steps (up to 500 nm) typically resulted in slightly thicker and rougher combed layers.

(31) Amimoto, S. T.; Force, A. P.; Gulotty, R. G., Jr.; Wiesenfeld, J. R. *J. Chem. Phys.* **1979**, *71*, 3640–7.

(32) Scoles, G., Ed. *Atomic and Molecular Beam Methods, Vol. 1*; Oxford University Press: New York and Oxford, U.K., 1988; 721 pp.

(33) Wang, Y.; Da, S.; Kim, M. J.; Kelly, K. F.; Guo, W.; Kittrell, C.; Hauge, R. H.; Smalley, R. E. *J. Am. Chem. Soc.* **2004**, *126*, 9502–3.

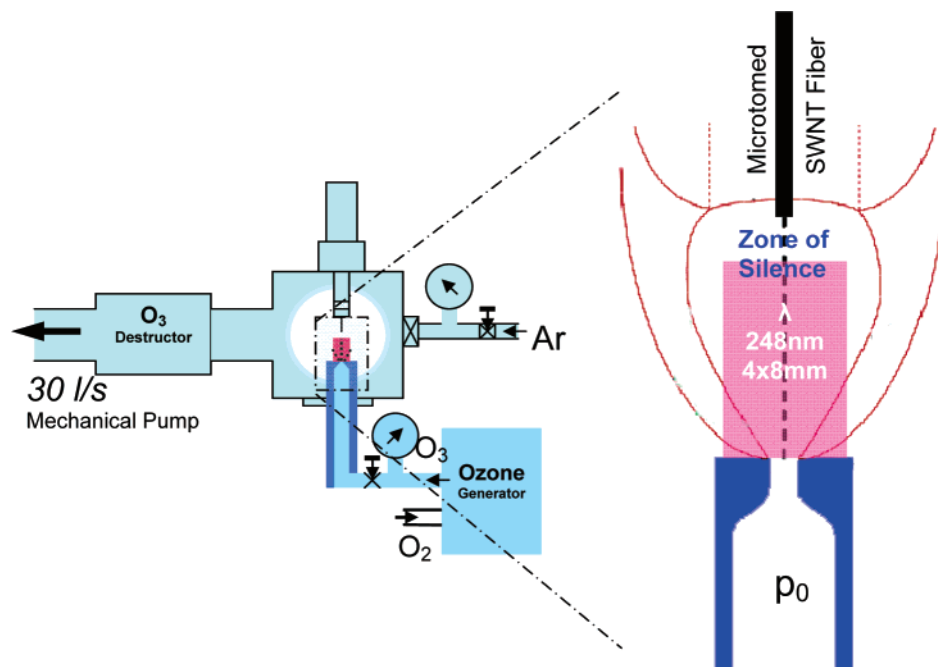


Figure 3. Schematic setup of a supersonic jet of atomic oxygen. The magnified drawing shows the “zone of silence” with respect to the laser beam and the fiber tip position. O_3 is first generated in an ozone generator and is then metered into a vacuum chamber. The residual O_3 is destroyed by hot copper wool before being pumped out. The microtomed fiber is mounted on a linear translator within the vacuum chamber. Atomic oxygen, responsible for the etching, is generated by focusing a KrF (248 nm) laser beam to dissociate gas-phase O_3 within the “zone of silence”, allowing the atomic oxygen diffusing to etch the combed layer.

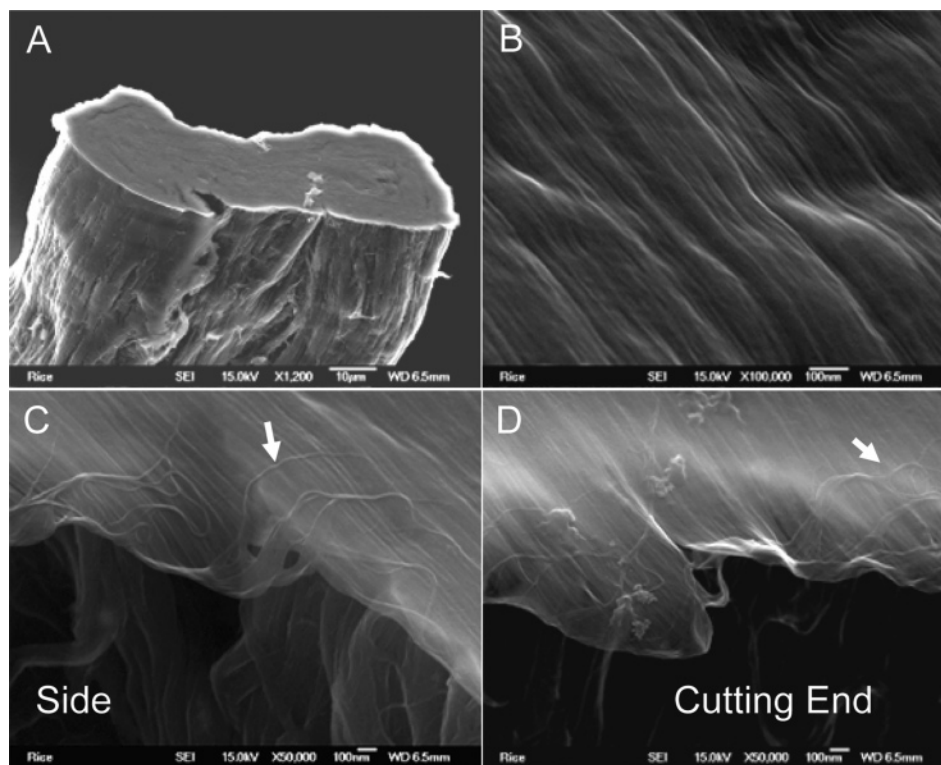


Figure 4. Scanning electron microscopy images of a microtomed SWNT neat fiber. (A) The dog-bone cross section of a 6% fiber. (B) SWNTs aligned along the microtoming direction to form a combed layer as thin as the diameter of a rope, as observed at the side (C) and the end of the combed layer (D).

Given the extreme hardness and sharpness (radius of curvature < 2 nm) of the diamond knife, this shearing effect constitutes a direct visualization of the exceptional toughness of SWNTs.^{6,7,34} Under the action of the diamond knife,

SWNTs at the fiber end were bent along the knife cutting direction but were not cut. Some SWNTs were pulled out of the fiber, probably because their length embedded in the fiber was sufficiently short that the van der Waals force was insufficient to balance the force applied by the knife. The phenomenon of shearing, but not cutting, is consistent with previous experiments³⁵ and simulations:³⁶ individual SWNTs

(34) Walters, D. A.; Ericson, L. M.; Casavant, M. J.; Liu, J.; Colbert, D. T.; Smith, K. A.; Smalley, R. E. *Appl. Phys. Lett.* **1999**, *74*, 3803–3805.

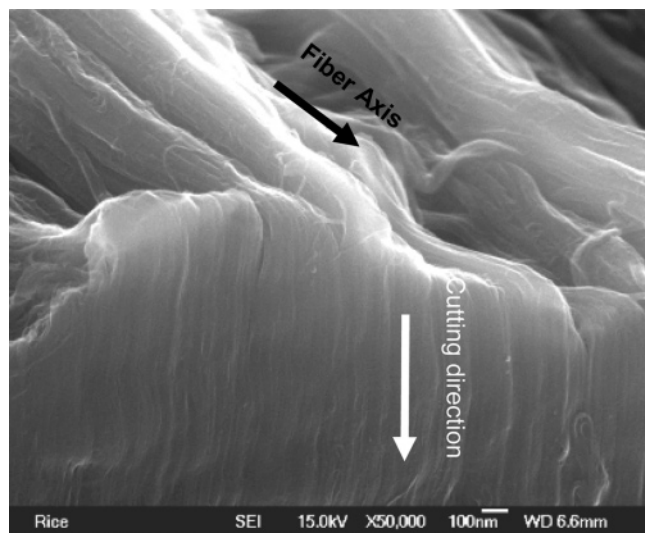


Figure 5. SEM image of the cut edge of a microtomed fiber. SWNTs were not cut but instead were bent along the cutting direction.

do not collapse or break easily, even if bent abruptly at a large angle. This parallels previous observations from a microtomed MWNT/epoxy composite at room temperature³⁷ as well as PBT fibers embedded in epoxy,³⁸ although PBT molecules are expected to bend more easily than SWNTs because their stiffness (or, equivalently, persistence length^{39,40}) is estimated to be 1–2 orders of magnitude lower.

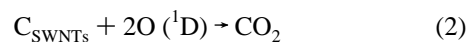
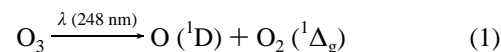
It is worth noting that the microtomed surface is smooth, making it easy to observe any morphology changes to the surface. This microtoming method allows slicing of the SWNT neat fiber, leading to ultrathin “in-plane” membranes of SWNTs⁴¹ with much better alignment than previous assembled materials.⁴² Finally, these microtomed samples provide ideal platforms for following chemical reactions of SWNTs, for example, continued growth of SWNTs⁴³ and supply-limited oxidation, to be discussed below.

3.2. Complimentary Oxygen Etching Approaches. To reveal the internal fiber structure, the combed layer must be removed. The well-aligned, thin, combed layer of SWNTs offered an ideal situation for addressing two important issues in SWNT chemistry: (1) What is the most efficient way to etch SWNT sidewalls? and (2) How can one selectively etch the nanotube ends? These two questions are directly related

to cutting^{44–46} and opening of SWNTs,^{47,48} essential steps for manipulation and derivatization of SWNTs.

Previous work on cutting long tubes into short pieces found that the sidewalls of SWNTs are relatively chemically inert.^{44,45,49} Often, SWNTs are shortened, rather than cut, indicating that the ends are more reactive than the sidewalls.⁵⁰ Because SWNTs in the combed layer have uneven starting positions (irregular beginnings and ends), etching from their ends would not yield a flat surface. Although some chemicals, such as a mixture of concentrated sulfuric and nitric acids, are capable of etching SWNT sidewalls, significant organic debris remains after the reaction.⁵⁰ In addition, the penetration of etching agents into the fibers is hard to avoid. Therefore, a wet chemistry approach is not ideal for removing the combed layer of SWNT ropes.

However, with a supersonic jet of O (¹D), the combed layer of SWNTs was etched away uniformly, indicating a dominant surface etching process. The etching rate was proportional to the flux of atomic oxygen and appeared approximately constant throughout the etching process. Such a proportional relationship was not found for O (³P). After the combed layer was completely removed, voids originally covered by the combed layer were revealed (Figure 6). The thickness of the removed combed layer was estimated from the side view SEM images to be 35 ± 15 nm. The molecular fluxes of O₃ and O (¹D) can also be calculated, following the well-established theory for supersonic jets³² and the photon dissociation of ozone³² (see Supporting Information). The balancing of these numbers reveals that O (¹D) etched SWNTs at an efficiency approaching stoichiometry; that is, every two O (¹D) striking the combed layer lead to the formation of a CO₂ following these equations:



This nearly stoichiometric efficiency indicates that O (¹D) etched SWNTs with virtually no differentiation between sidewalls and ends, despite the lower susceptibility of the sidewalls. Because of the high reactivity of O (¹D), etching was limited to the surface, preventing roughening or pitting. Interestingly, the high etching efficiency also suggests that O (¹D) survives the shock wave around the tip of the fiber, probably owing to the small size of the fiber (~30–100 μm in diameter).

- (35) Iijima, S.; Brabec, C.; Maiti, A.; Bernholc, J. *J. Chem. Phys.* **1996**, *104*, 2089–92.
- (36) Yakobson, B. I.; Brabec, C. J.; Bernholc, J. *J. Comput.-Aided Mater. Des.* **1996**, *3*, 173–182.
- (37) Ajayan, P. M.; Stephan, O.; Colliex, C.; Trauth, D. *Science* **1994**, *265*, 1212–14.
- (38) Cohen, Y.; Thomas, E. L. *Macromolecules* **1988**, *21*, 433–5.
- (39) Yakobson, B. I. In *Handbook of Nanoscience, Engineering and Technology*; Goddard, W. A. I., Brenner, D. W., Lyshevsk, S. E., Iafate, G. J., Eds.; CRC Press: Boca Raton, FL, 2003.
- (40) Mark, J. E. *Polymer Data Handbook*; Oxford University Press: New York, 1999.
- (41) Wang, Y. Seed Crystals and Catalyzed Epitaxy of Single Walled Carbon Nanotubes. Ph.D. Thesis, Rice University, Houston, TX, 2004.
- (42) Walters, D. A.; Casavant, M. J.; Qin, X. C.; Huffman, C. B.; Boul, P. J.; Ericson, L. M.; Haroz, E. H.; O’Connell, M. J.; Smith, K.; Colbert, D. T.; Smalley, R. E. *Chem. Phys. Lett.* **2001**, *338* (1), 14–20.
- (43) Wang, Y.; Kim, M. J.; Shan, H.; Kittrell, C.; Fan, H.; Ericson, L. M.; Hwang, W.-F.; Arepalli, S.; Hauge, R. H.; Smalley, R. E. *Nano Lett.* **2005**, *5*, 997–1002.

- (44) Liu, J.; Rinzler, A. G.; Dai, H. J.; Hafner, J. H.; Bradley, R. K.; Boul, P. J.; Lu, A.; Iverson, T.; Shelimov, K.; Huffman, C. B.; Rodriguez-macias, F.; Shon, Y. S.; Lee, T. R.; Colbert, D. T.; Smalley, R. E. *Science* **1998**, *280*, 1253–1256.
- (45) Gu, Z.; Peng, H.; Hauge, R. H.; Smalley, R. E.; Margrave, J. L. *Nano Lett.* **2002**, *2*, 1009–1013.
- (46) Lustig, S. R.; Boyes, E. D.; French, R. H.; Gierke, T. D.; Harmer, M. A.; Hietpas, P. B.; Jagota, A.; McLean, R. S.; Mitchell, G. P.; Onoa, G. B.; Sams, K. D. *Nano Lett.* **2003**, *3*, 1007–1012.
- (47) Hornbaker, D. J.; Kahng, S. J.; Misra, S.; Smith, B. W.; Johnson, A. T.; Mele, E. J.; Luzzi, D. E.; Yazdani, A. *Science* **2002**, *295*, 828–831.
- (48) Luzzi, D. E.; Smith, B. W. *Carbon* **2000**, *38*, 1751–1756.
- (49) Ziegler, K. J.; Gu, Z.; Peng, H.; Flor, E. L.; Hauge, R. H.; Smalley, R. E. *J. Am. Chem. Soc.* **2005**, *127*, 1541–1547.
- (50) Kuznetsova, A.; Popova, I.; Yates, J. T., Jr.; Bronikowski, M. J.; Huffman, C. B.; Liu, J.; Smalley, R. E.; Hwu, H. H.; Chen, J. G. *J. Am. Chem. Soc.* **2001**, *123* (43) 10699.

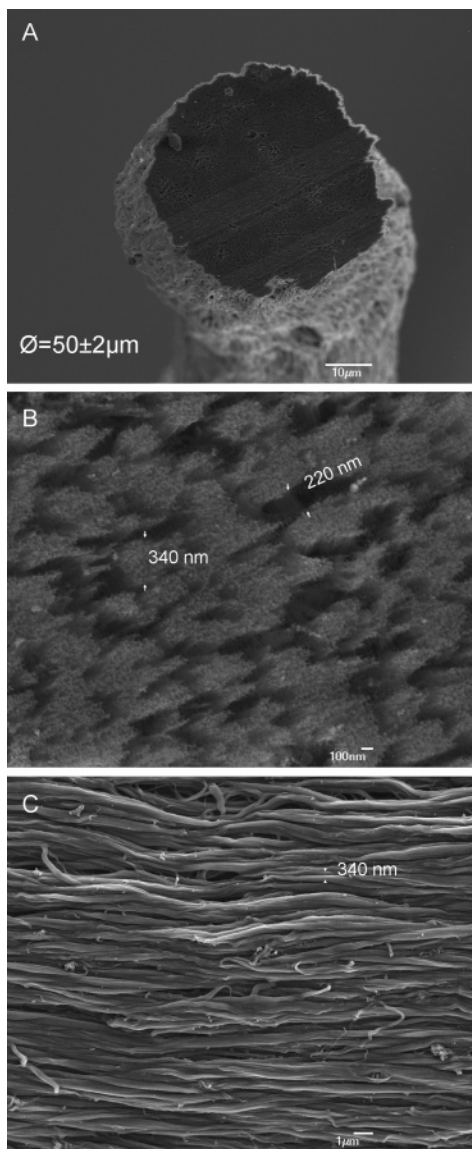


Figure 6. SEM images showing (A) the relatively uniform circular cross-section of a SWNT fiber spun from a 10 wt % dispersion of SWNTs in 102% H_2SO_4 . The cross section was revealed by microtoming, followed by etching with O (1D). (B) After the combed layer was completely etched away, the internal voids (dark) and fibril structures (light) were revealed. These fibril structures show the same diameters as observed on the skin of the fiber (C).

In contrast to O , O_2 was found to etch preferably from the ends, rather than from the sidewalls. The two etching modes can be easily identified by examining the morphological changes. O_2 at elevated temperatures was very aggressive. After heating at 900–960 °C in 0.50 Torr of O_2 for 30 min, SWNT ropes completely transformed into chains of graphitic carbon particles or micrometer-sized graphite. The transformation is clearly a coordinated reaction involving SWNTs that were in contact. While large ropes were transformed into graphitic carbon particles, individuals and small bundles remained visible in SEM images.

However, by lowering O_2 pressure to a supply-limited regime, etching was restricted to the surface. After a combed layer was etched with 1.5 mTorr O_2 at 900 °C for 30 min, no graphite particles were observed. A fibrous network was left behind, with the gaps and voids exposed (Figure 7). The initially continuous combed layer became short segments;

many ends were visible with bright particles, presumably oxidized metal catalyst particles from the HiPco growth process, located at their ends. These patterns indicate that O_2 primarily etched SWNTs from their ends, yielding a nonuniform length distribution due to the position and length distribution of individual SWNTs in the starting fiber. The resulting irregular etching excludes O_2 as a preferred method for the removal of the combed layer.

However, we found that trace amounts of O_2 etched the fiber from the outside in, uniformly exposing the internal structures of SWNT fibers. For example, Figure 8 shows that the diameter of a 10% fiber decreased from $50 \pm 2 \mu\text{m}$ to $\sim 37 \mu\text{m}$ after oxidation. The well-preserved shape and the homogeneity of the fiber's diameter suggest uniform etching. The etched fiber shows substructures well-aligned along the fiber axis but with decreased sizes due to oxidation. These observations confirmed that the internal structure in our spun fibers were essentially the same as on the fiber's surface. Compared to other methods, such as peeling, this oxidation method is free of any mechanical artifacts and therefore provides a reliable method for investigating the fiber's internal structure.

3.3. Substructures of SWNT Neat Fibers and Their Origins. Both the surface morphology and the analysis of the internal structures of SWNT neat fibers revealed a substructure of aligned SWNT superropes approximately 200–500 nm in diameter. This substructure is observed as a dominant feature both on the fiber skin (Figure 6C) and in the interior after the combed layer was completely removed (Figure 6) or the skin was etched away by the supply-limited oxidation method (Figure 8). Often, these superropes weave in and out along the fiber axis but appeared to be “endless” (above 500 μm long) and uniform in diameter along their length. The substructure was uniform throughout the SWNT neat fibers, a significant difference from other nanotube fibers, such as composite SWNT/poly(vinyl alcohol) (PVA) fibers, which form a skin–core structure with a well-aligned, denser skin encasing a porous, disordered interior.^{16,19}

The uniform substructures showed that the coagulation of a 6–10 wt % dope in an ether coagulation bath could occur uniformly. From the etched cross section, a packing density of $70\% \pm 15\%$ for the 10 wt % fiber can be determined. This number is in fairly good agreement with the packing density, 81%, that can be derived by directly converting the SWNT mass in the dope to a solidified neat fiber of diameter $50 \pm 2 \mu\text{m}$, assuming no drawing or thinning of the 10 wt % (or 13.2 vol %) SWNT/ H_2SO_4 dope upon leaving the 125 μm needle orifice. The good agreement between the two numbers suggests a simple picture for the current fiber spinning process: little extension occurs after the dope leaves the needle. This is consistent with a fiber spinning process without an air gap between the needle and the coagulation bath (wet spinning). Spinning poly(*p*-phenyleneterephthalamide) (PPTA, commercialized under Kevlar) or poly(*p*-phenylenebenzobisoxazole) (PBO, Zylon) with an air gap allows further alignment of the polymers, a key element for successful dry-jet wet-spinning of aramid fibers.⁵¹ The air gap effect on the spinning of SWNT fibers is an interesting challenge for further exploration.

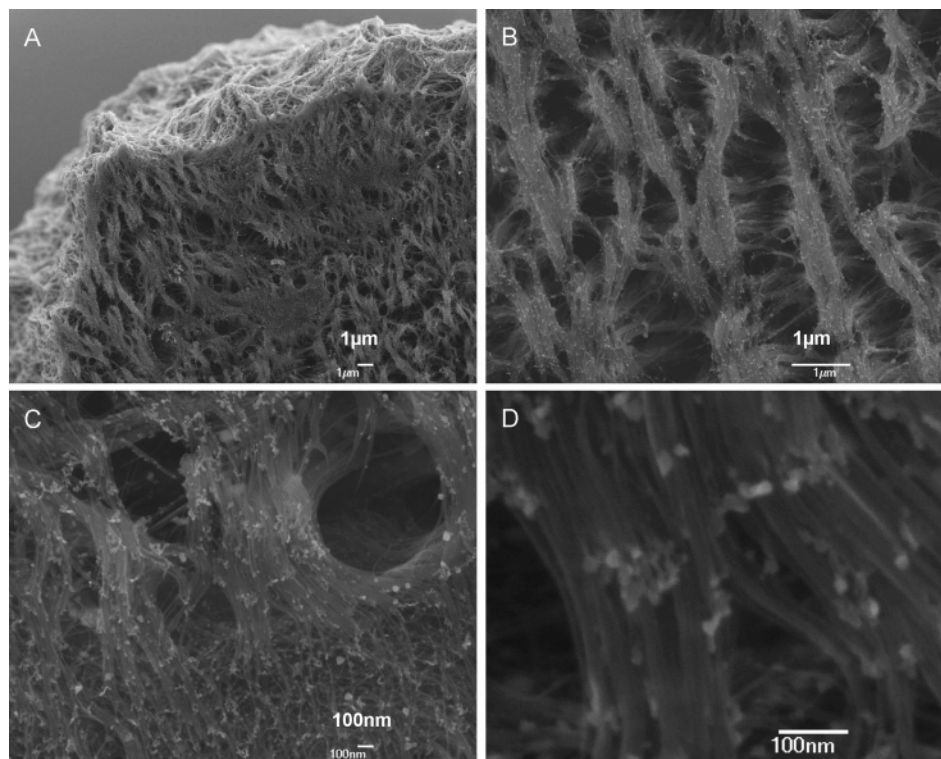


Figure 7. SEM images (A to D in successively increasing magnification) showing the fibrous network of a combed layer that were partially etched with an O₂ supply-limited oxidation strategy. The SWNT combed layer was etched with 1.5 mTorr oxygen at 900 °C (laser heating) for 20 min.

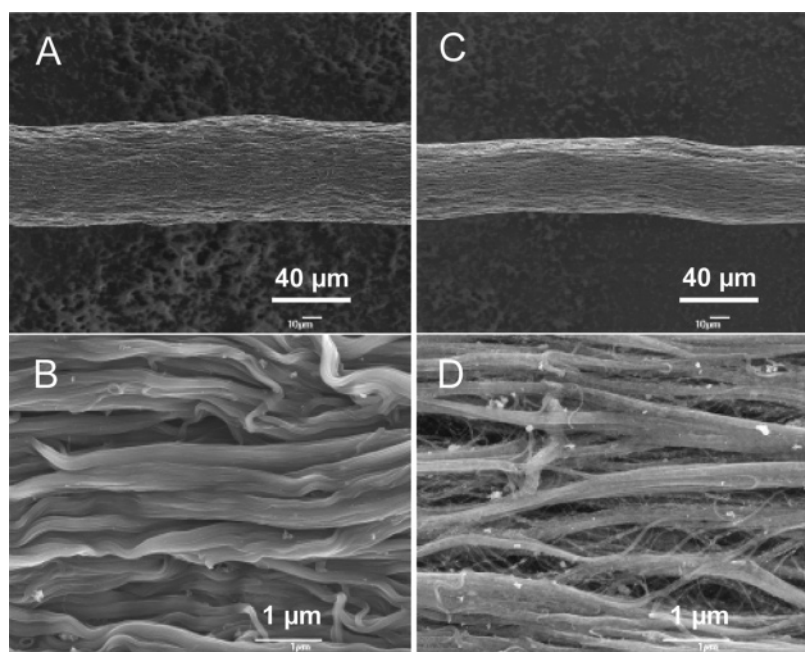


Figure 8. Oxygen supply-limited oxidation reveals internal alignment in a 10 wt % SWNT fiber (A, B) before and (C, D) after the oxidation.

In an effort to understand the extrusion and coagulation process, additional neat SWNT fibers were spun from a custom mixer/extruder.²³ Similar superrope substructures were observed in fibers spun from SWNT/H₂SO₄ dispersions from a range of starting concentrations (6–10 wt %) and varying coagulation conditions, including two different coagulating baths (diethyl ether and dilute H₂SO₄) and different bath temperatures (0 and 25 °C).

These superrope substructures may be linked to the morphology of the dope from which the fibers are spun. At concentrations between about 0.1 and 1 wt %, SWNT/H₂SO₄ dispersions show a unique morphology composed of threadlike domains (dubbed SWNT spaghetti) of aligned SWNTs associated with acid in equilibrium with a low-concentration isotropic phase of randomly oriented SWNTs in acid.²² SWNTs are highly aligned and mobile along the axis of the spaghetti, which appear endless and have a diameter below 600 nm (diffraction limit of the optical

(51) Gupta, V. B.; Kothari, V. K. *Manufactured Fiber Technology*; 1997; 664 pp.

microscope). The unusual structure of the spaghetti phase may be due to a balance of short-range repulsion (induced by protonation³⁰ and dependent on Hammett acidity⁵²) and long-range attraction (induced by van der Waals forces) between SWNTs, as well to the SWNT stiffness, which would tend to favor bend defects (compatible with a threadlike structure) and suppress splay and twist (necessary for the formation of spherical domains). However, it is still unclear whether the spaghetti morphology persists at concentrations greater than 1 vol %, because above this concentration SWNT/acid dispersions become opaque and show polydomain liquid crystalline morphology,^{22,53} which prevents the direct identification of individual spaghetti domains.

These observations reveal an intriguing similarity between the superropes in the fibers and the SWNT spaghetti phase: the SWNT superropes found in the solid fibers may be the result of direct coagulation of SWNT spaghetti structures preexisting in the liquid dope. However, fibrillar structures have been observed in fibers spun from liquid crystalline dopes of rodlike polymers that form globular (rather than spaghetti-like) domains, for example, PBO in polyphosphoric acid;⁵⁴ therefore, more evidence on the structure of the high concentration (6–10 wt %) dopes used for spinning is needed before final conclusions can be made.

4. Conclusions

We have developed the experimental means to directly visualize the internal voids, alignment, and composition of neat SWNT fibers. The methods include a special microtoming technique, which allowed the accurate determination

of the cross section, and two complementary etching methods to reveal the internal structures without mechanical artifacts. Because of the toughness of SWNTs, the microtoming produced a flat surface with a well-aligned, ultrathin combed layer of SWNT ropes. These well-structured combed layers provided a unique surface for exploring the SWNT chemistry. With an O (¹D) supersonic jet, the combed layer was etched uniformly at nearly stoichiometric efficiency, indicating that O (¹D) etches a SWNT from both the ends and the sidewall. In contrast, under supply-limited thermal oxidation conditions, SWNTs were consumed primarily from the ends. These two distinct etching modes allowed either complete removal of the combed layer or etching through the skin layer by layer to directly visualize the internal structures.

Both the analysis of the internal structures and the surface morphology of SWNT neat fibers revealed a substructure of aligned SWNT superropes approximately 200–500 nm in diameter. This substructure was observed as a dominant feature throughout both the fiber and the skin and may be linked to the morphology of the starting liquid crystalline phase.

Acknowledgment. We acknowledge discussions with Virginia Davis, Nick Parra-Vasquez, Pradeep Rai, Wen-Fang Hwang, Gerry Lavin, Bruce Brinson, Paul Ruchhoeft, Jack Wolfe, Wei Zhou, and Jack Fischer. This work was supported by the U.S. Department of Energy (DE-AC05-000R22725), the Office of Naval Research under the DURINT program (N00014-01-1-0789), and by the Robert A. Welch Foundation (C-0689). Y.W. gratefully acknowledges a David G. Nance Award from Nanotechnology Foundation in Texas and a Rice Presidential Fellowship.

Supporting Information Available: Calculations of the etching efficiency of SWNTs using a supersonic jet of atomic oxygen (PDF). This material is available free of charge via the Internet at <http://pubs.acs.org>.

CM0518473

(52) Davis, V. A. Phase Behavior and Rheology of Single-Walled Carbon Nanotubes (SWNTs) in Superacids with Application to Fiber Spinning. PhD Thesis, Rice University, Houston, TX, 2005.

(53) Zhou, W.; Heiney, P. A.; Fan, H.; Smalley, R. E.; Fischer, J. E. *J. Am. Chem. Soc.* **2005**, *127*, 1640–1641.

(54) Cohen, Y.; Adams, W. W. *Polymer* **1996**, *37*, 2767–2774.